

First data set of H₂O/HDO columns from TROPOMI

Andreas Schneider¹, Tobias Borsdorff¹, Joost aan de Brugh¹, Franziska Aemisegger², Dietrich G. Feist^{3,4,5}, Rigel Kivi⁶, Frank Hase⁷, Matthias Schneider⁷, and Jochen Landgraf¹

¹Earth science group, SRON Netherlands Institute for Space Research, Utrecht, the Netherlands

²Atmospheric Dynamics group, Department of Environmental Systems Science, ETH Zürich, Zürich, Switzerland

³Ludwig-Maximilians-Universität München, Lehrstuhl für Physik der Atmosphäre, Munich, Germany

⁴Deutsches Zentrum für Luft- und Raumfahrt, Institut für Physik der Atmosphäre, Oberpfaffenhofen, Germany

⁵Max Planck Institute for Biogeochemistry, Jena, Germany

⁶Finnish Meteorological Institute, Sodankylä, Finland

⁷Institute of Meteorology and Climate Research (IMK-ASF), Karlsruhe Institute of Technology, Karlsruhe, Germany

Correspondence: Andreas Schneider (a.schneider@sron.nl)

Abstract. Global measurements of atmospheric water vapour isotopologues aid to better understand the hydrological cycle and improve global circulation models. This paper presents a new data set of vertical column densities of H₂O and HDO retrieved from short-wave infrared (2.3 μ m) reflectance measurements by the Tropospheric Monitoring Instrument (TROPOMI) aboard the Sentinel-5 Precursor satellite. TROPOMI features daily global coverage with a spatial resolution of up to 7 km \times 7 km.

5 The retrieval utilises a profile-scaling approach. The forward model neglects scattering, thus strict cloud filtering is necessary. For validation, recent ground-based water vapour isotopologue measurements by the Total Carbon Column Observing Network (TCCON) are employed. A comparison of TCCON δ D with ground-based measurements by the project Multi-platform remote Sensing of Isotopologues for investigating the Cycle of Atmospheric water (MUSICA) for data prior to 2014 (where MUSICA data is available) shows a bias in TCCON δ D estimates. As TCCON HDO is currently not validated, an overall correction of 10 recent TCCON HDO data is derived based on this finding. The agreement between the corrected TCCON measurements and collocated TROPOMI observations is good with an average bias of $(-0.2 \pm 3) \cdot 10^{21}$ molec cm⁻² ($(1.0 \pm 7.4) \%$) in H₂O and $(-2 \pm 7) \cdot 10^{17}$ molec cm⁻² ($(-1.2 \pm 7.4) \%$) in HDO, which corresponds to a bias of $(-14 \pm 18) \%$ in a posteriori δ D. The use of the data set is demonstrated with a case study of a blocking anticyclone in northwestern Europe in July 2018 using single overpass data.

15 1 Introduction

Atmospheric water vapour represents the strongest natural greenhouse gas and transports a large amount of energy through latent heat and thus plays a fundamental role in shaping weather and climate (Kiehl and Trenberth, 1997; Harries, 1997). However, uncertainties in the quantification of these two effects are still large and represent one of the key uncertainties in current climate prediction (Stevens and Bony, 2013). To improve on that requires new observations on a global scale and with 20 a long-term perspective. To this end, satellite observations from space are considered as the most promising approach (Rast et al., 2014).

Constraints for the hydrological cycle are offered by observations of isotopologues of water vapour. Different equilibrium vapour pressures and diffusion constants of different isotopologues lead to isotopic fractionation whenever a phase change occurs. Isotopic fractionation is associated with a partitioning of the heavy and light isotopologues in the different phases, which 25 depends on the thermodynamic conditions of the environment. The relative abundance of a heavy isotopologue with respect to the light isotopologue in an air parcel is therefore dependent on the source region's temperature and relative humidity, the source water's isotopic composition as well as the entire transport history of the air parcel, including all evaporation, condensation and mixing events (e. g. Dansgaard, 1964; Craig and Gordon, 1965). This makes measurements of water vapour isotopologues a unique diagnostic of the hydrological cycle (Dansgaard, 1964) and a valuable benchmark for the evaluation and 30 further development of global and regional circulation models (e. g. Joussaume et al., 1984; Hoffmann et al., 1998; Yoshimura et al., 2008; Risi et al., 2010; Pfahl et al., 2012).

The usual notation to describe the isotopological abundance variations is the relative difference of the ratio of the heavy and the light isotopologue, here HDO and H_2O , $R_D = c_{\text{HDO}}/c_{\text{H}_2\text{O}}$, to a standard abundance ratio $R_{\text{D, std}}$,

$$\delta D = \frac{R_D - R_{\text{D, std}}}{R_{\text{D, std}}} \quad (1)$$

35 (Coplen, 2011). The commonly used standard ratio is Vienna Standard Mean Ocean Water (VSMOW), $R_{\text{D, std}} = 3.1152 \times 10^{-4}$.

Measurements of atmospheric water vapour isotopologues are not very common. In situ observations are performed from aircrafts and balloons (e. g. Rinsland et al., 1984; Dyroff et al., 2010, 2015; Herman et al., 2014; Sodemann et al., 2017) and on the ground (e.g. Wen et al., 2010; Aemisegger et al., 2012; Bastrikov et al., 2014) using laser spectrometers or cryogenic trapping techniques. Remote sensing instruments exist on the ground and on space or balloon based platforms. The former 40 are usually Fourier transform infrared (FTIR) spectrometers. Ground stations are often organised in networks. The largest networks are the Total Carbon Column Observing Network (TCCON, Wunch et al., 2011) and the Network for the Detection of Atmospheric Composition Change (NDACC, De Mazière et al., 2018). The data product of the former includes H_2O and HDO, while for measurements by the latter water vapour isotopologues are retrieved by the project Multi-platform remote Sensing of Isotopologues for investigating the Cycle of Atmospheric water (MUSICA, Schneider et al., 2016). From satellites, 45 H_2O and HDO were first retrieved by Zakharov et al. (2004) using thermal infrared measurements from the Interferometric Monitor for Greenhouse gases (IMG) sensor aboard the Advanced Earth Observing Satellite (ADEOS). Later, this was followed by the Tropospheric Emission Spectrometer (TES) on the Earth Observing System (EOS) Aura satellite (Worden et al., 2006), the Michelson Interferometer for Passive Atmospheric Sounding (MIPAS) aboard European Space Agency (ESA)'s environmental satellite (ENVISAT) (Steinwagner et al., 2007; Payne et al., 2007), the SCanning Imaging Absorption spectroMeter for Atmospheric CHartographY (SCIAMACHY) instrument on ENVISAT (Frankenberg et al., 2009; Scheepmaker et al., 2015; Schneider et al., 2018), the Infrared Atmospheric Sounding Interferometer (IASI) aboard the MetOP satellite (Herbin et al., 2009; Schneider and Hase, 2011; Schneider et al., 2016; Lacour et al., 2012), the Greenhouse Gases Observing Satellite (GOSAT) (Frankenberg et al., 2013; Boesch et al., 2013), and the Atmospheric Infrared Sounder (AIRS) on board the NASA Aqua satellite (Worden et al., 2019). The sensitivity of instruments observing in the thermal infrared (IMG, TES, 50 MIPAS, IASI, AIRS) is very different from that of instruments measuring in the short-wave infrared like SCIAMACHY and

GOSAT. While the former are mainly sensitive in the stratosphere and free troposphere, the latter have good sensitivity in the lower troposphere including the boundary layer. On 13th October 2017, the Tropospheric Monitoring Instrument (TROPOMI) aboard the Sentinel-5 Precursor (S5P) satellite (Veenkind et al., 2012) was launched. It has a short-wave infrared band in heritage of SCIAMACHY with a spectral range of 2305–2385 nm and a spectral resolution of 0.25 nm, yet with a signal to noise ratio much better than SCIAMACHY and an unprecedented spatial resolution of 7 km \times 7 km (in the centre of the swath). This work presents a new data set of H₂O and HDO columns from TROPOMI observations starting at first light of the instrument on 9th November 2017. Section 2 introduces the retrieval method. Section 3 presents a ground-based data set to validate the satellite observations against, and the comparison between both data sets is shown in Section 4. Section 5 provides a first insight into the data set's use for studying synoptic-scale variability in the atmospheric branch of the water cycle. Finally, the 65 summary of the results and the conclusions are given in Section 6.

2 Retrieval method

The retrievals are performed with the short-wave infrared retrieval algorithm SICOR, which utilises a profile-scaling approach and is described in detail by Scheepmaker et al. (2016); Landgraf et al. (2016); Borsdorff et al. (2014). Below, the most important features are summarised and the specific setup is given.

70 Using the spectral window from 2354.0 nm to 2380.5 nm (Scheepmaker et al., 2016), the algorithm fits the total columns of H₂O, HDO, CH₄ and CO together with a Lambertian surface albedo in the form of an order 1 Legendre polynomial. The isotopologue H₂¹⁸O is included in the forward model but not fitted. A priori profiles of water vapour are adapted from the European Centre for Medium-Range Weather Forecasts (ECMWF) analysis product. Since the ECMWF data product does not distinguish individual isotopologues, H₂O, HDO and H₂¹⁸O profiles are obtained from the water vapour profile by scaling it 75 with the respective average relative natural abundances. That implicitly corresponds to a prior of δD of 0 %. A priori profiles of CH₄ and CO are taken from TM5 simulations (Krol et al., 2005). Scattering cross-sections are taken from HITRAN 2016 (Gordon et al., 2017). The forward model ignores scattering, so that strict filtering for clear-sky scenes is necessary. To this end, collocated measurements from the Visible Infrared Imaging Radiometer Suite (VIIRS) instrument aboard the Suomi National 80 Polar-orbiting Partnership (S-NPP) satellite, which flies in formation with S5P, are used (Siddans, 2016). The cloud cover threshold is 1 % for both inner field of view and outer field of view. Moreover, soundings with high aerosol load are filtered out by a two-band filter as introduced by Scheepmaker et al. (2016); Hu et al. (2018), which in the present configuration requires that the ratio of retrieved methane in bands with weak and strong absorption (2310–2315 nm and 2363–2373 nm, respectively) is between 0.94 and 1.06. Furthermore, scenes with solar zenith angle greater than 75° are discarded because they are prone to errors due to more scattering and diffraction effects which are not covered well by the forward model and due to typically low 85 radiances meaning low signal-to-noise ratio.

An exemplary spectral fit and the resulting residuals (which are defined as measured minus modelled radiances) are shown in Fig. 1. The root mean square (rms) residual (cyan horizontal line in panel (b)) is in the order of the rms uncertainty of the radiance (purple horizontal line).

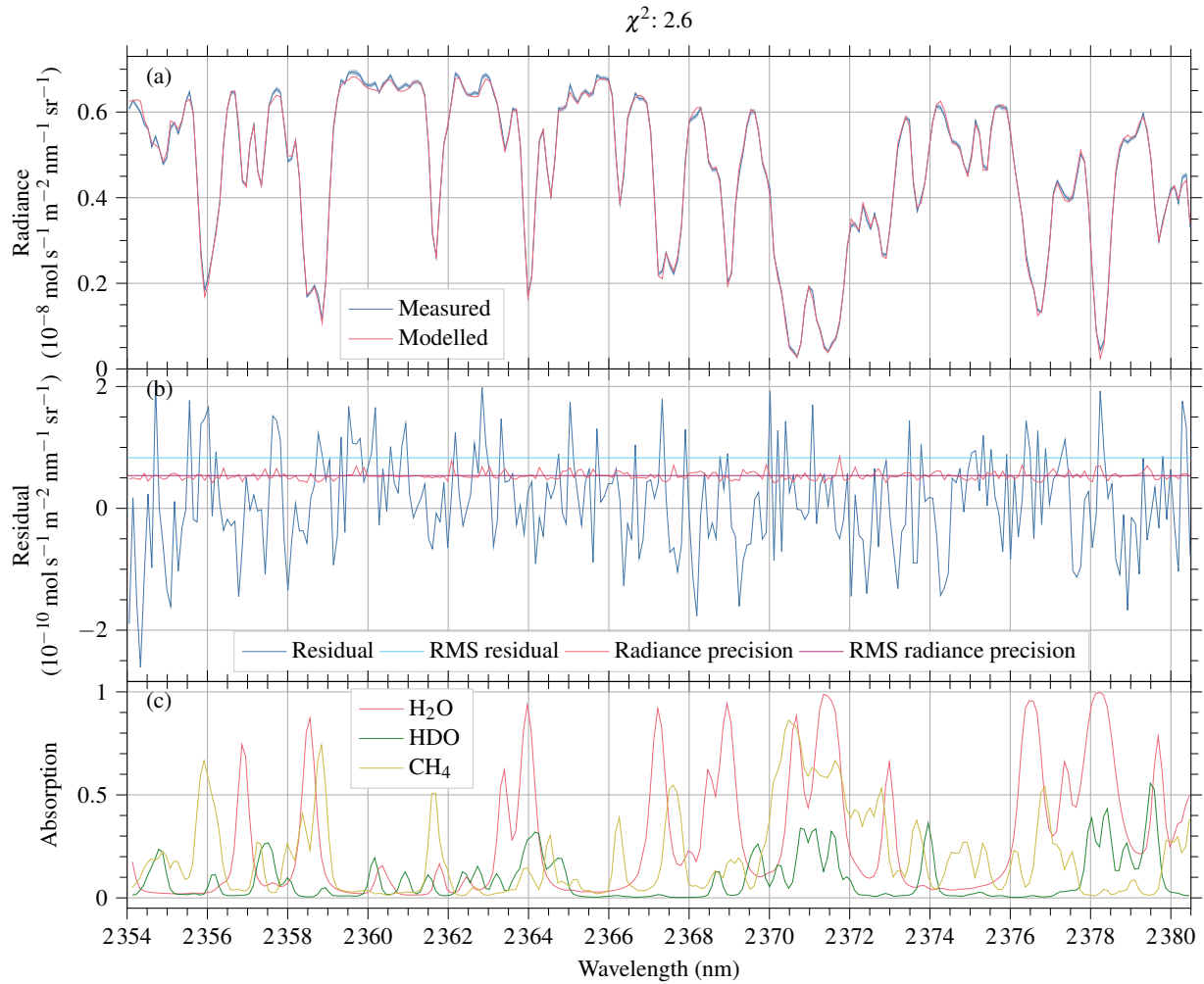


Figure 1. (a) Measured radiance (blue) with its precision (light blue band) and spectral fit (red) for ground pixel 149129 in orbit 3969 located near Wollongong, Australia on 20 Jul 2018. (b) Corresponding residuals (defined as measured minus modelled radiances, blue) and its root mean square (rms, cyan), precision of the radiance (red) and its rms (purple). (c) Simulated absorption by H_2O (red), HDO (green) and CH_4 (yellow).

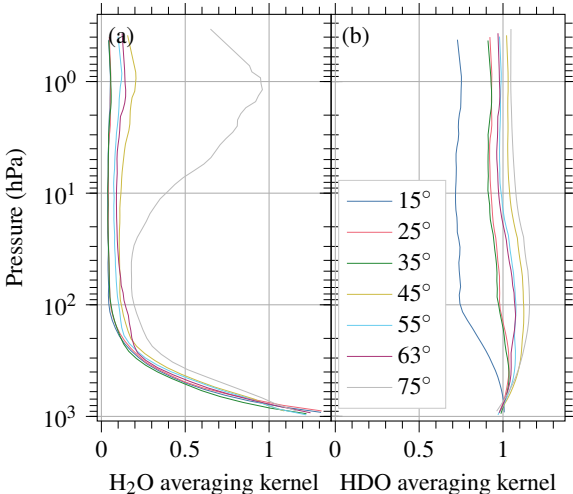


Figure 2. Examples of column averaging kernels for (a) H₂O and (b) HDO for different solar zenith angles in orbit 4924 on 25 Sep 2018.

The sensitivity of a retrieved column to changes in a given altitude region is described by the column averaging kernel (Rodgers, 2000). The ideal averaging kernel is unity in all altitudes, but in practice the sensitivity changes with height. Figure 2 depicts examples of column averaging kernels for different solar zenith angles. The sensitivity for the two isotopologues are significantly different. For H₂O, the highest sensitivity is in the lowest layer (where typically most water vapour resides) and decreases with increasing altitude. The sensitivity in the stratosphere is small, however the amount of water vapour in this altitude region is very small and contributes little to the total column. The sensitivity of HDO does not deviate as much from unity as the one of H₂O. In the lower troposphere it increases slightly with increasing altitude until reaching a maximum depending on solar zenith angle, above which it decreases. The differences in column averaging kernel are due to the different absorption strength of the two isotopologues and mean that a posteriori δD is sensitive on the profile shapes, particularly of the main isotopologue H₂O since for that the averaging kernel deviates considerably from unity in higher altitudes.

3 Ground-based FTIR data sets

To validate the TROPOMI retrievals, ground-based Fourier transform infrared (FTIR) measurements are used. HDO is a product of NDACC-MUSICA (Barthlott et al., 2017) and TCCON (Wunch et al., 2015). NDACC-MUSICA provides two products: type 1 is the direct retrieval output, and type 2 contains a posteriori processed output which reports the optimal estimation of {H₂O, δD } pairs; here the type 2 product is used because it is recommended for isotopologue analyses (Barthlott et al., 2017). Seven stations are in both networks: Eureka, Ny Ålesund, Bremen, Karsruhe, Izaña, Wollongong and Lauder. This allows to compare the TCCON and NDACC-MUSICA (here type 2) data products, which reveals a large difference in δD of on average 58 % (which corresponds to a mean relative difference of -30%) when collocating with a maximal time difference of one

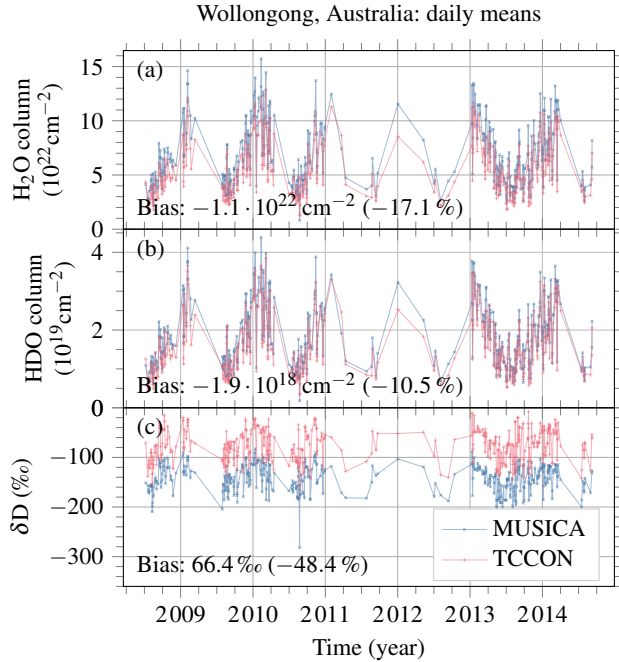


Figure 3. Time series of daily averages of H_2O (a), HDO (b) and a posteriori δD (c) of the NDACC-MUSICA type 2 (blue crosses) and TCCON (red pluses) data products at Wollongong, Australia. The bias in δD without daily averaging is 65.8 ‰ (−47.4 ‰).

hour. An example for Wollongong is plotted in Fig. 3. A comparison between MUSICA and TCCON has also been performed by Weaver (2019). He compares the MUSICA type 1 product with TCCON and finds a bias in δD of on average 40 ‰.

MUSICA is explicitly created for isotopologue studies, and δD profiles have been validated against aircraft measurements in 110 an altitude range of 2–7 km during a dedicated campaign in summer 2013 (Schneider et al., 2015; Dyroff et al., 2015; Schneider et al., 2016). However, data is only available until 2014, so that there is no temporal overlap with TROPOMI which has been launched in October 2017. TCCON H_2O total columns are calibrated with in situ measurements (mainly radiosondes); a so-called aircraft correction factor of 1.0183 is applied to match the reference (Wunch et al., 2015). However, TCCON HDO is currently not verified and so no correction factor is applied to it. Thus it is assumed that TCCON HDO has to be corrected.

115 In order to correct for the discrepancy, the idea is to scale TCCON HDO to match MUSICA δD . Scaling HDO with a factor a , i. e. $c_{\text{HDO}} \mapsto ac_{\text{HDO}}$, is equivalent to the linear transformation

$$\delta\text{D} \mapsto a \delta\text{D} + a - 1 \quad (2)$$

in δD . Figure 4a depicts a correlation histogram of TCCON δD vs. MUSICA δD for the station Wollongong. Here, the relation between MUSICA and TCCON is to a good degree described by a simple scaling of the column. The result of a fit of Eq. (2) to 120 the data is plotted as blue line, giving the scaling factor for the TCCON HDO column. To demonstrate that this approach does not involve intercept issues, a linear fit of slope and intercept (red line) together with the confidence interval computed with

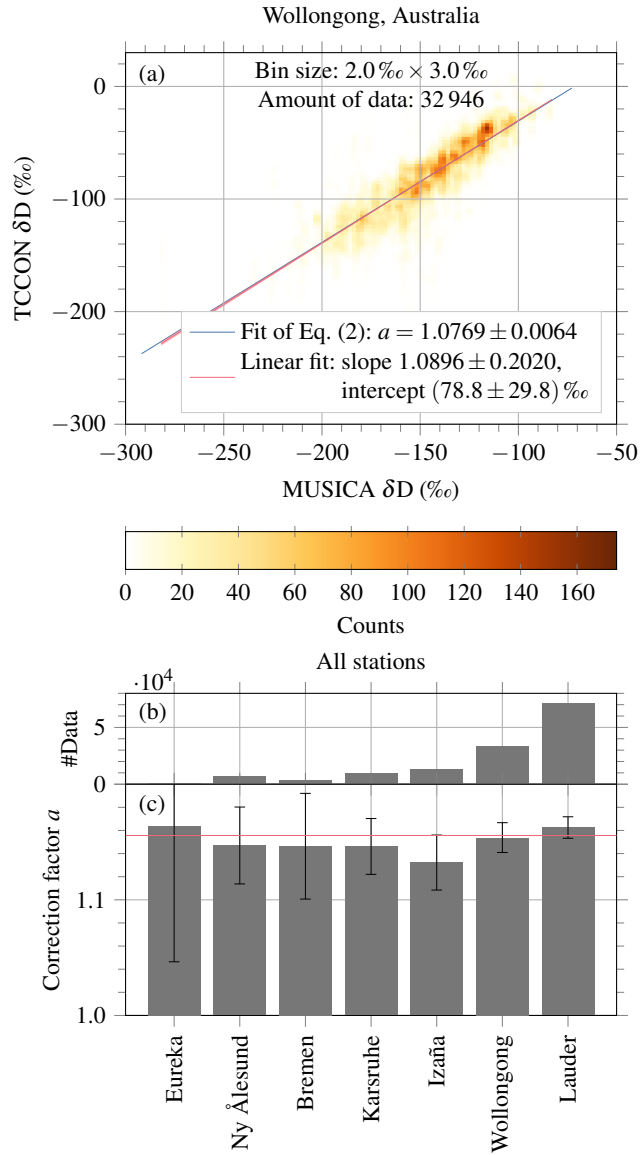


Figure 4. (a) Exemplary correlation histogram of TCCON δD vs. MUSICA δD for Wollongong, Australia. The blue line shows the result of a fit of Eq. (2), giving the correction factor for TCCON HDO. The red line shows a linear fit with slope and intercept, the red shading its confidence interval computed with the bootstrap method. (b) Amount of collocated measurements for all stations in both networks. (c) Fit results of correction factors for individual stations. The red line corresponds to the error-weighted average over all stations, $a = 1.0778$.

the bootstrap method (i. e. by 10 000 times fitting a randomly reduced data set, red shading) has also been plotted in the figure. Both slope and offset are similar to the approach with Eq. 2, and the latter lies within the confidence band of the former. The bar chart in Fig. 4c visualises fit results for all stations in both networks. It shows that the correction factor does not change 125 much between stations. The large difference in fit error is mostly due to the large difference in the amount of data (Fig. 4b). Thus it is meaningful to scale HDO at all TCCON stations by the error-weighted average correction factor $a = 1.0778$ in order to correct TCCON's bias in HDO and thus δD .

Table 1. List of TCCON stations used for the validation.

Station	Latitude	Longitude	Altitude	Data available from/to	Reference
Eureka	80.1° N	86.4° W	610 m	24 Jul 2010–15 Aug 2019	Strong et al. (2019)
Sodankylä	67.4° N	26.6° E	190 m	16 May 2009–22 Sep 2019	Kivi et al. (2014)
East Trout Lake	54.4° N	105.0° W	500 m	07 Oct 2016–02 Jun 2019	Wunch et al. (2018)
Bialystok	53.2° N	23.0° E	190 m	01 Mar 2009–29 Sep 2018	Deutscher et al. (2015)
Bremen	53.1° N	8.9° E	30 m	22 Jan 2010–27 Sep 2018	Notholt et al. (2014)
Karlsruhe	49.1° N	8.4° E	110 m	19 Apr 2010–02 Jul 2019	Hase et al. (2015)
Paris	48.8° N	2.4° E	60 m	23 Sep 2014–27 Sep 2018	Té et al. (2014)
Orléans	48.0° N	2.1° E	130 m	29 Aug 2009–29 Sep 2018	Warneke et al. (2019)
Park Falls	45.9° N	90.3° W	440 m	02 Jun 2004–03 Jun 2019	Wennberg et al. (2017)
Rikubetsu	43.5° N	143.8° E	380 m	16 Nov 2013–26 Sep 2018	Morino et al. (2018b)
Lamont	36.6° N	97.5° W	320 m	06 Jul 2008–02 Jun 2019	Wennberg et al. (2016)
Tsukuba	36.0° N	140.1° E	30 m	04 Aug 2011–28 Sep 2018	Morino et al. (2018a)
Edwards	35.0° N	117.9° W	700 m	20 Jul 2013–02 Jun 2019	Iraci et al. (2016)
JPL	34.2° N	118.2° W	390 m	19 May 2011–14 May 2018	Wennberg et al. (2014)
Pasadena	34.1° N	118.1° W	240 m	20 Sep 2012–01 Jun 2019	Wennberg et al. (2015)
Saga	33.2° N	130.3° E	10 m	28 Jul 2011–30 Mar 2019	Kawakami et al. (2014)
Wollongong	34.4° S	150.9° E	30 m	25 Jun 2008–29 Sep 2018	Griffith et al. (2014)
Lauder	45.0° S	169.7° E	370 m	02 Feb 2010–03 Apr 2019	Sherlock et al. (2014); Pollard et al. (2019)

4 Validation of TROPOMI retrievals

For validation, TROPOMI observations are collocated with TCCON measurements with a radius of 30 km, a maximal altitude 130 difference of 500 m, a field of view of 45° in the FTIR viewing direction and a maximal time difference of 2 h. Here, the TCCON HDO data are corrected according to the approach presented in the previous section. Table 1 gives an overview of all stations used. Other stations have too few (less than 5 days) collocated measurements and have thus not been included in the validation study. No altitude correction is applied here. The mentioned collocation criterion for altitude is used to ensure that no bias due to large height difference between station and satellite ground pixel is introduced (cf. Schneider et al., 2018). For each

135 station, daily averages are computed over all collocated measurements. Figure 5 shows an exemplary time series for Edwards. The collocated observations of H_2O and HDO agree very well, and the agreement in δD is also good with more scatter and a small bias. Corresponding correlation plots are depicted in Fig. 6. Panels (a) and (b) confirm the excellent agreement in H_2O and HDO with a Pearson correlation coefficient of 0.99, and a corresponding correlation coefficient of 0.96 for δD . The average difference between TROPOMI and TCCON defines the bias. In δD , a small bias is plain in the correlation plot and
140 amounts to -23\% .

Fig 7 depicts the validation statistics for all TCCON stations. The correlation in H_2O and HDO is high for all stations. In δD , the correlation is high except for a lower correlation of 0.60 at Lauder and a low correlation of 0.37 at Saga. At these stations the variability in δD is small, but H_2O and HDO vary considerably. At Saga the amount of data is very small. Fig. 8 shows the biases. The bias in H_2O and HDO is small with an average over all stations of $-2 \cdot 10^{20} \text{ molec cm}^{-2}$ (corresponding to a
145 relative bias of 1.0 \%) for H_2O and $-2 \cdot 10^{17} \text{ molec cm}^{-2}$ (-1.2\%) for HDO . The mean bias in δD is -14\% or 6 \%, which is good taken into account that δD is very sensitive to small errors in H_2O or HDO .

5 Demonstration of applications of the data set

An illustration of the TROPOMI retrievals on the global and monthly scale is depicted in Fig. 9 for September 2018. There is no data over the oceans because water is too dark in the short-wave infrared and glint measurements are not taken into account.
150 The data gaps in tropical regions are due to persistent clouds. The data quality in terms of noise is significantly better than for a multi-year average of SCIAMACHY observations, cf. Schneider et al. (2018, Fig. 7). In the spatial distribution shown in Fig. 9 the major isotopic effects formulated by Dansgaard (1964) can be recognised. The general latitudinal gradient due to the temperature-dependence of the fractionation effects and progressive rain out of heavy isotopologues, the so-called latitudinal effect, is clearly visible. The continental effect of depletion due to rain out of the heavy isotopologue is visible on all continents
155 including Australia. The altitude effect, which describes depletion above high ground due to lower temperature and increasing rain out, can be seen, for example, over the Andes and the Himalayas.

To demonstrate the quality and the possibilities of the new data set of water vapour isotopologues from TROPOMI, a case study using single overpass results over Europe on 30th July 2018 is presented in Fig. 10. The summer 2018 was one of the hottest and driest in central and northern Europe (Copernicus Climate Service, 2018; Gubler et al., 2018) with forest
160 fires in Scandinavia, dry fields and low river stages all over the central and northern parts of the continent. The reason for this exceptionally hot and dry summer was the presence of a high pressure system over northern Europe that blocked the otherwise predominant westerly moist flow from the North Atlantic. Synoptic-scale atmospheric blocking situations can lead to hot temperature extremes due to adiabatic warming of the descending air in the core of the anticyclone (Pfahl and Wernli, 2012). The descending vertical motion favours clear sky conditions and thus further contributes to the surface warming through
165 radiative effects in the centre of the anticyclone (Trigo et al., 2004). In particular, the end of July 2018 was characterised by a stationary blocking anticyclone extending over the entire troposphere over northwestern Russia and Scandinavia. This blocking led to large-scale descent and to a divergent flow near the surface in its core, resulting in clear sky conditions over northwestern

Armstrong Flight Research Center, Edwards, CA, USA

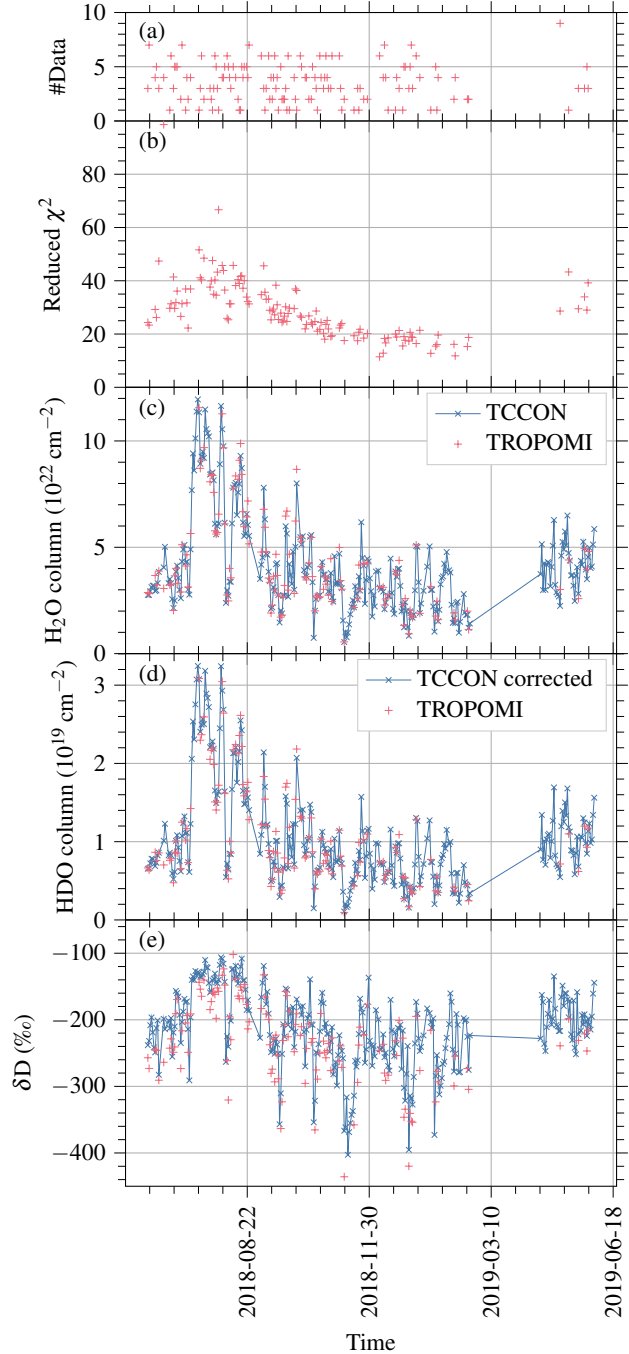


Figure 5. Time series of daily averages of corrected TCCON measurements (blue crosses) and collocated TROPOMI observations (red pluses) at Edwards (34.96° N, 700 m a. s. l.). Shown are (a) the number of individual observations per day, (b) Reduced χ^2 , (c) H_2O columns, (d) HDO columns, and (e) a posteriori δD .

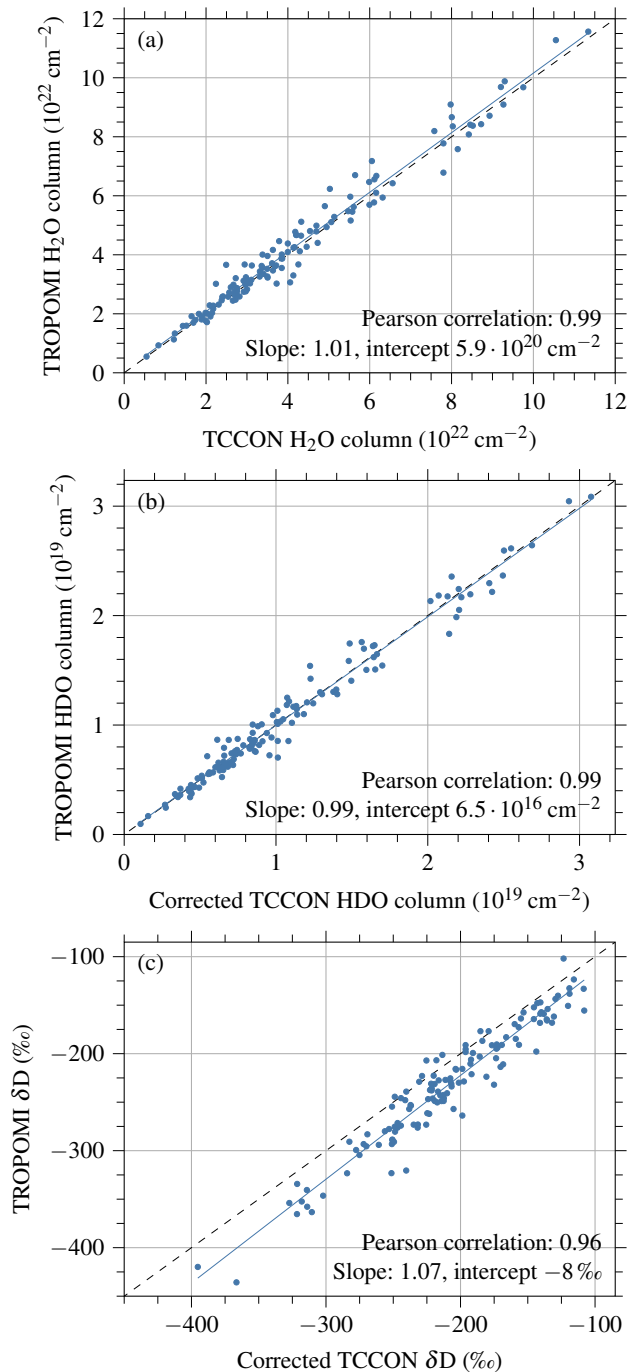


Figure 6. Correlation plot of corrected TCCON measurements and collocated TROPOMI observations for Edwards for daily averages of H_2O columns (a), HDO columns (b), and δD (c). The dashed lines mark equality, the solid lines give linear fits to the data.

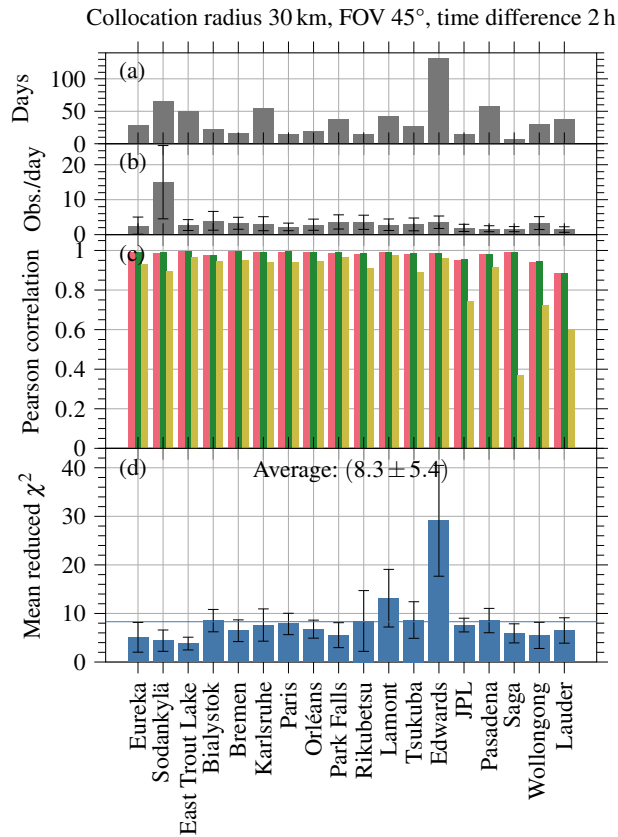


Figure 7. Statistics of the validation for all TCCON stations. **(a)** Number of days with collocated measurements. **(b)** Average number of collocated TROPOMI observations per day with its standard deviation. **(c)** Pearson correlation coefficient for H₂O (red), HDO (green) and δD (yellow). **(d)** Average reduced χ^2 and its standard error; the blue line visualises the average over all stations.

Russia and Finland (see Fig. 10c). The isotopic signature of the blocking anticyclone in Fig. 10b reflects this synoptic flow configuration with low δD signals of between -250‰ and -200‰ in the centre of the anticyclone. The depleted total column vapour in this region is due to the large-scale subsidence bringing depleted (Fig. 10b) and dry (Fig. 10d) upper tropospheric air towards lower levels. The near-surface divergent wind exports more enriched freshly evaporated moisture that is taken up near the surface towards the edges of the blocking. The anticyclone area is characterised by clear skies (Fig. 10c) with low specific humidity ($1\text{--}3\text{ g kg}^{-1}$ at 700 hPa, Fig. 10d), low relative humidity (10–30 % at 700 hPa, Fig. 10e) and high potential temperature associated with the dry subsiding (adiabatically warming) air masses (Fig. 10f). The dry low-level outflow encounters moister and warmer air at the edge of the surface anticyclone, leading to a very strong horizontal gradient of specific and relative humidity (Fig. 10d,e) in the lower troposphere. As a consequence the warm moist air is forced to rise, localised instabilities occur and isolated convective cells develop leading to condensation and the formation of a ring of clouds around the blocking anticyclone. A distinct arc-like feature of enriched total column water vapour at the edge of the anticyclone can be distinguished

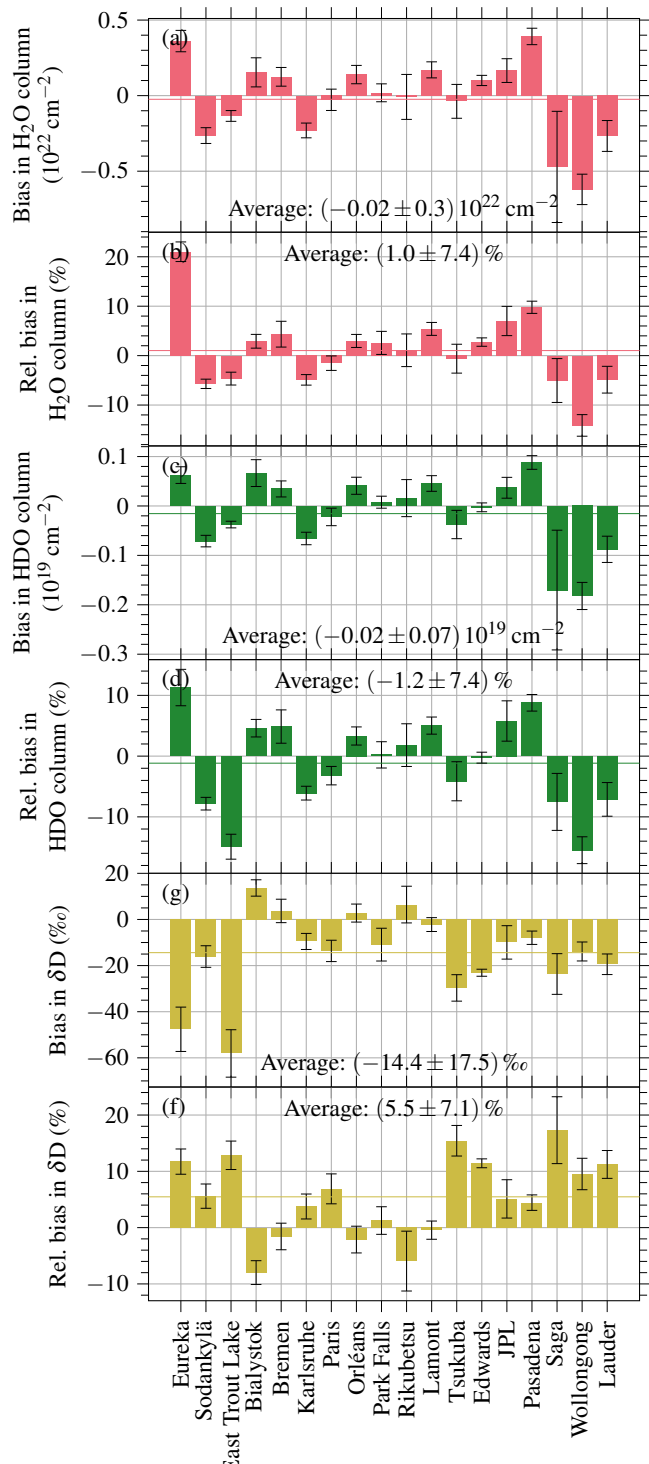


Figure 8. Biases for all TCCON stations. **(a)** Bias in H₂O and its standard error. **(b)** Relative bias in H₂O and its standard error. **(c)** Bias in HDO and its standard error. **(d)** Relative bias in HDO and its standard error. **(e)** Bias in a posteriori δD and its standard error. **(f)** Relative bias in a posteriori δD and its standard error. The horizontal line in all panels visualises the average over all stations.

01 Sep 2018 to 30 Sep 2018

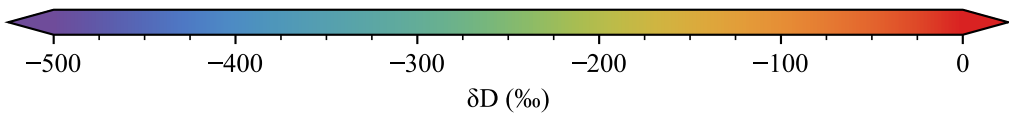
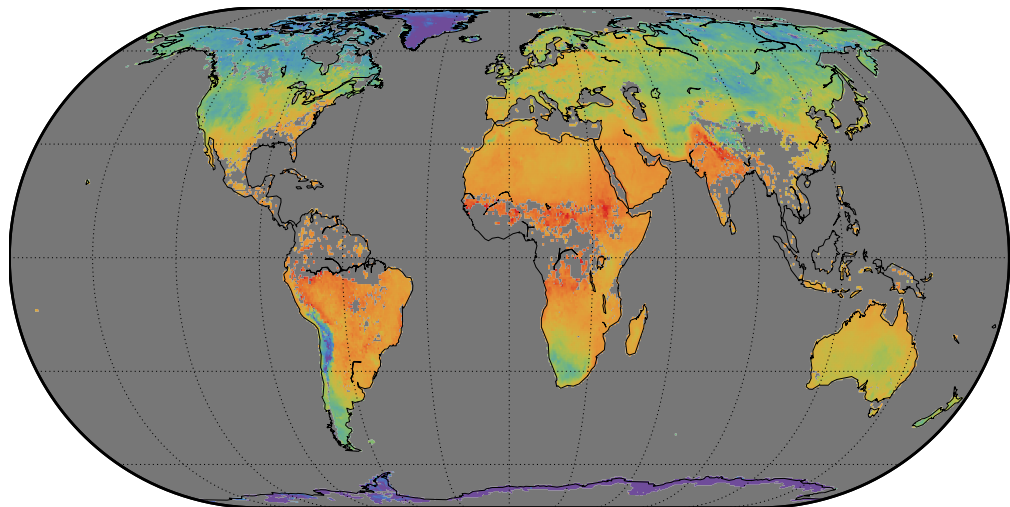
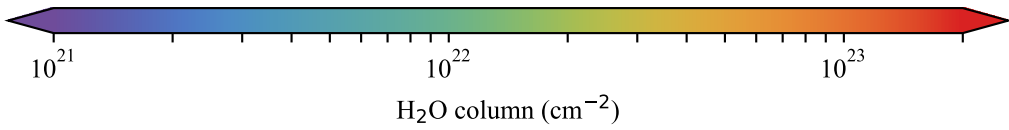
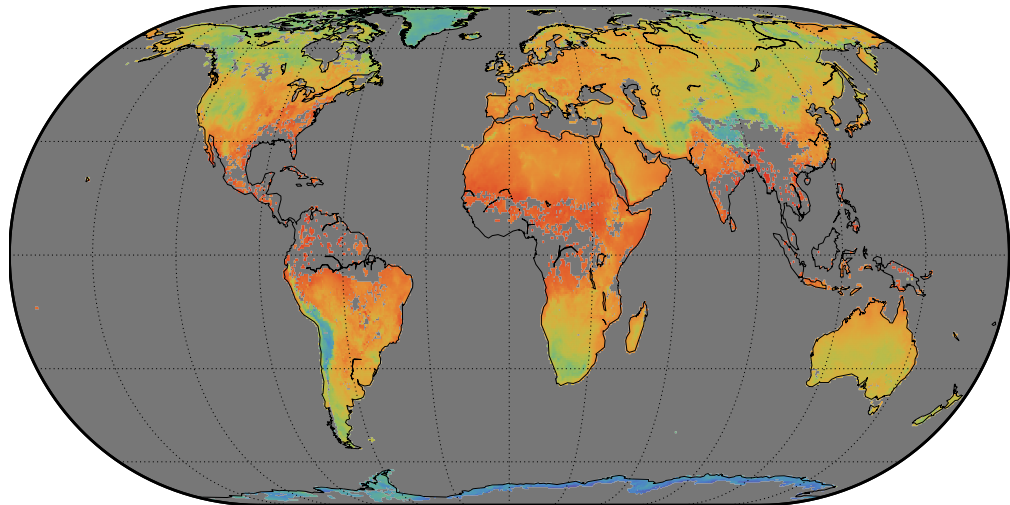


Figure 9. Global plots of H₂O (a) and δD (b) averaged over September 2018 on a grid of $0.5^\circ \times 0.5^\circ$. The average of δD is weighted with the H₂O column for mass conservation purposes.

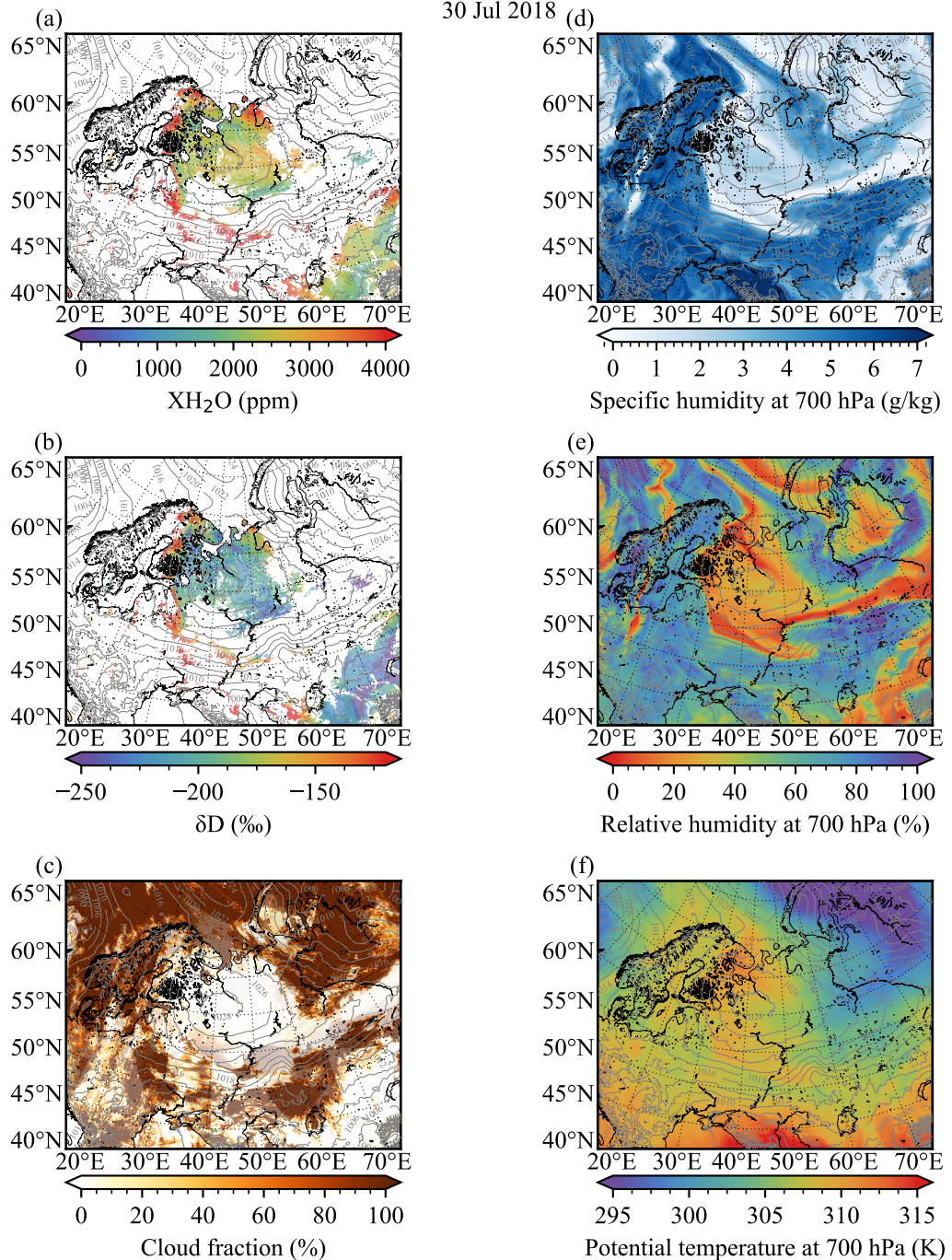


Figure 10. TROPOMI single overpass results for H_2O column (a) and δD (b) over Europe on 30 Jul 2018; VIIRS cloud fraction on the same day (c); specific humidity (d), relative humidity (e), and potential temperature (f) at 700 hPa from the ECMWF analysis product over Europe at 12:00 UTC on 30 Jul 2018. The 700 hPa level is chosen for the thermodynamic variables because it reflects the large-scale conditions in the lower troposphere above the continental boundary layer. The overlaying contours in all panels show mean sea-level pressure from ECMWF at 12:00 UTC with a contour line distance of 2 hPa.

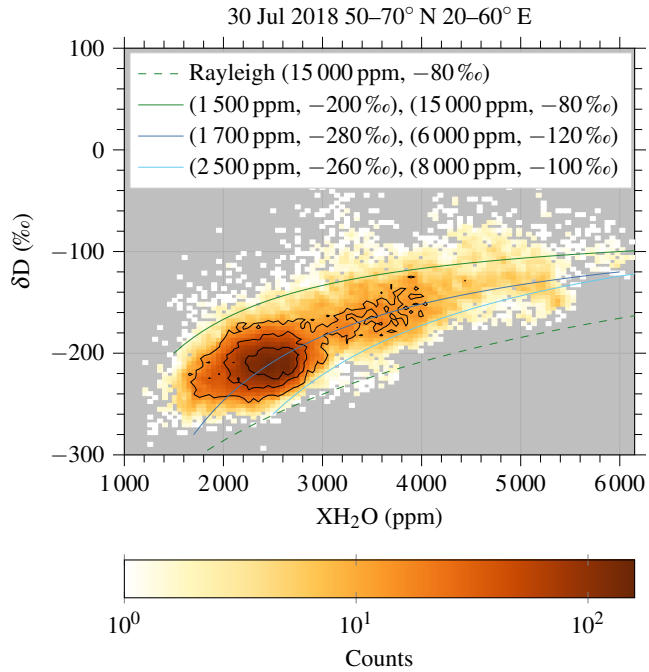


Figure 11. Two-dimensional histogram of all TROPOMI observations in the area 50–70° N, 20–60° E on 30 Jul 2018 (colour-coded). The black contours show 25 %, 50 % and 75 % levels of the cumulative density. The dashed green curve represents a Rayleigh fractionation process, the solid green, blue and cyan curves represent idealised mixing processes as specified by the legend.

slightly displaced from the first clouds in the northwest (Fig. 10b). Turbulent mixing and convection injecting more enriched, 180 freshly evaporated moisture advected with the large-scale flow from marine environments (Barents Sea, North Sea and Black Sea) could be the reason for this interesting enriched ring-like water vapour isotopologue pattern. A very depleted cloud free area south of the Ob river with δD values below -250 ‰ (Fig. 10b) might be connected to anomalously strong subsidence of northerly continental air masses.

The large range of measured δD and H_2O mixing ratios during the northeastern European blocking on 30th July 2018 185 (Fig. 10a, b) becomes apparent in Fig. 11, where a two-dimensional histogram and the cumulative density of the TROPOMI data in the region 50–70° N and 20–60° E is shown together with two different types of idealised scenarios of airmass transformation (coloured lines). These simple idealised scenarios are frequently used in the literature to guide the interpretation of stable isotope measurements in H_2O – δD diagrams (e. g. Rozanski and Sonntag, 1982; Worden et al., 2007; Noone, 2012). The first scenario illustrated by the dashed green line in Fig. 11 is that an air parcel with a humidity of 15 000 ppm and $\delta\text{D} = -80\text{ ‰}$ 190 (typical for the continental boundary layer in this northerly continental region, Bastrikov et al., 2014) experienced moist adiabatic ascent with condensation following a Rayleigh process (dashed green line, Rayleigh, 1902; Dansgaard, 1964). The progressive decrease of δD with decreasing water vapour mixing ratio would thus be due to preferential condensation of HDO compared to H_2O and subsequent removal of hydrometeors by precipitation. The dashed green Rayleigh curve in Fig. 11 shows

195 a behaviour that is different from the TROPOMI data points. Given the clear sky conditions and the subsidising movement of the air masses within the blocking anticyclone, the assumptions needed for a Rayleigh distillation process are hardly fulfilled. The second scenario illustrated by the solid green, blue, and cyan lines is that two air parcels with distinct humidity and δD are mixed due to turbulent and convective mixing to yield different blends that follow the so-called mixing lines in the H_2O - δD space. The highest density of observed blocking anticyclone points retrieved by TROPOMI is located in the region spanned by the green and the cyan mixing lines in the H_2O - δD space. The 25 %, 50 % and 75 % contours of cumulative density of points 200 are aligned with the blue mixing line. This suggests that a two end-member mixing process describes the data much better than an idealised Rayleigh process (dashed green line in Fig. 11). In this particular synoptic situation, this corresponds to the moistening of a subsidising air mass from the mid troposphere.

In future work, the nature and occurrence of these features should be analysed in more detail including a catalogue of different continental blocking events with observations from TROPOMI.

205 Apart from investigations on the water cycle dynamics associated with continental blockings, many other dynamically interesting contexts exist where TROPOMI could present an important added value for further investigations. These comprise among others the region of the heat low over the Sahara (e. g. Schneider et al., 2015; González et al., 2016; Lacour et al., 2017) or continental regions upstream of cold air surges leading to events of strong ocean evaporation along the warm ocean western boundary currents (Aemisegger and Papritz, 2018; Aemisegger and Sjolte, 2018).

210 6 Summary and conclusions

This work presents a new data set of H_2O and HDO columns retrieved from TROPOMI short-wave infrared observations. Scattering is ignored in the forward model so that a strict cloud filtering is necessary, which is performed with collocated VIIRS measurements. The data quality is such that single overpasses yield meaningful results, which is a huge step forward compared to previous missions like SCIAMACHY.

215 For validation of the TROPOMI data product, particular attention must be given to the reference data sets. At this stage, there are two data products of ground-based observations of the HDO total column available, provided by the TCCON and NDACC-MUSICA networks. Comparing these two data products for stations in both networks reveals a large bias between the ground-based products of on average 58 % in δD . NDACC-MUSICA was decidedly developed for water vapour isotopologue studies and is validated in δD with aircraft measurements, but data are only available until 2014. TCCON provides recent 220 data with temporal overlap with TROPOMI observations and its H_2O total column data product is validated against in situ measurements, however its HDO data product is not verified. In order to obtain a suitable validation data set, TCCON HDO columns are scaled by a factor of 1.0778 to match the MUSICA δD over the common observation time period.

Using a collocation radius of 30 km, a maximal altitude difference of 500 m, a field of view of 45° and a maximal time difference of 2 h, a good agreement between corrected TCCON measurements and collocated TROPOMI observations is found. 225 The mean bias is $(-0.2 \pm 3) \cdot 10^{21} \text{ molec cm}^{-2}$ ($(1.0 \pm 7.4) \%$) for H_2O , $(-2 \pm 7) \cdot 10^{17} \text{ molec cm}^{-2}$ ($(-1.2 \pm 7.4) \%$) for HDO , and $(-14 \pm 18) \%$ ($(5.5 \pm 7.1) \%$) for δD .

The use of the new data set is demonstrated in a case study of an atmospheric blocking event with a single TROPOMI overpass over northeastern Europe on 30th July 2018. Depleted air masses are found in the core of the anticyclone due to subsidence bringing upper tropospheric air towards lower levels. At the edge of the anticyclone a ring of enriched air is 230 observed. A climatological study on the water vapour isotopic signature of continental summer blocking events could provide promising insights into the atmospheric water cycling associated with such systems that frequently lead to heat waves and hot temperature extremes. This case study shows the quality of the new data set and the added value for isotopologue studies, enabling studies on a day-by-day basis with high spatial resolution over continental regions.

Due to the restrictive filter for clear sky scenes, the data coverage is limited. To improve on this, cloudy-sky retrievals over 235 low clouds will be considered in a future work by using a forward model that accounts for scattering. Moreover, a calibration and validation of the TCCON HDO product is necessary. Additionally, it would be beneficial if recent NDACC-MUSICA data would become available. Finally, an improvement in the consistency between the networks would be very valuable.

Data availability. The TROPOMI HDO data set of this study is available for download at ftp://ftp.sron.nl/open-access-data-2/TROPOMI/tropomi/hdo/9_1/. TCCON data are available from the TCCON Data Archive at <https://tccondata.org/>. MUSICA data are available from 240 <ftp://ftp.cpc.ncep.noaa.gov/ndacc/MUSICA/>.

Author contributions. Andreas Schneider, Tobias Borsdorff, Joost aan de Brugh and Jochen Landgraf made the TROPOMI HDO retrievals and the analysis. Franziska Aemisegger carried out the case study in Section 5. Dietrich G. Feist aided in the search for the cause of discrepancies between (uncorrected) TCCON HDO and TROPOMI HDO. Rigel Kivi and Frank Hase provided TCCON data. Matthias Schneider provided MUSICA data and TCCON data. All authors discussed the results and commented on the manuscript.

245 *Competing interests.* The authors declare that they have no conflict of interest.

Disclaimer. Plots/data contain modified Copernicus Sentinel data, processed by SRON.

Acknowledgements. This work was supported by the ESA Living Planet Fellowship project Water vapour Isotopologues from TROPOMI (WIFT). The TROPOMI data processing was carried out on the Dutch national e-infrastructure with the support of the SURF Cooperative. The project MUSICA has been funded by the European Research Council under the European Community's Seventh Framework Programme 250 (FP7/2007–2013)/ERC grant agreement number 256961. KIT acknowledges BMWi for funding TCCON data analysis and delivery through DLR project 50EE1711A. The TCCON project for the Tsukuba site is supported in part by the GOSAT series project. Nicholas Deutscher,

David Griffith, Laura T. Iraci, Isamu Morino, Justus Notholt, Christof Petri, Dave Pollard, Kei Shiomi, Kimberly Strong, Yao Té, Thorsten Warneke, Paul Wennberg and Debra Wunch provided TCCON data.

References

255 Aemisegger, F. and Papritz, L.: A Climatology of Strong Large-Scale Ocean Evaporation Events. Part I: Identification, Global Distribution, and Associated Climate Conditions, *J. Climate*, 31, 7287–7312, <https://doi.org/10.1175/JCLI-D-17-0591.1>, 2018.

Aemisegger, F. and Sjolte, J.: A Climatology of Strong Large-Scale Ocean Evaporation Events. Part II: Relevance for the Deuterium Excess Signature of the Evaporation Flux, *J. Climate*, 31, 7313–7336, <https://doi.org/10.1175/JCLI-D-17-0592.1>, 2018.

260 Aemisegger, F., Sturm, P., Graf, P., Sodemann, H., Pfahl, S., Knohl, A., and Wernli, H.: Measuring variations of $\delta^{18}\text{O}$ and $\delta^2\text{H}$ in atmospheric water vapour using two commercial laser-based spectrometers: an instrument characterisation study, *Atmos. Meas. Tech.*, 5, 1491–1511, <https://doi.org/10.5194/amt-5-1491-2012>, 2012.

Barthlott, S., Schneider, M., Hase, F., Blumenstock, T., Kiel, M., Dubravica, D., García, O. E., Sepúlveda, E., Mengistu Tsidu, G., Takele Keene, S., Grutter, M., Plaza-Medina, E. F., Stremme, W., Strong, K., Weaver, D., Palm, M., Warneke, T., Notholt, J., Mahieu, E., Servais, C., Jones, N., Griffith, D. W. T., Smale, D., and Robinson, J.: Tropospheric water vapour isotopologue data (H_2^{16}O , H_2^{18}O , and HD^{16}O) as obtained from NDACC/FTIR solar absorption spectra, *Earth Syst. Sci. Data*, 9, 15–29, <https://doi.org/10.5194/essd-9-15-2017>, 2017.

265 Bastrikov, V., Steen-Larsen, H. C., Masson-Delmotte, V., Gribanov, K., Cattani, O., Jouzel, J., and Zakharov, V.: Continuous measurements of atmospheric water vapour isotopes in western Siberia (Kourovka), *Atmos. Meas. Tech.*, 7, 1763–1776, <https://doi.org/10.5194/amt-7-1763-2014>, 2014.

270 Blumenstock, T., Hase, F., Schneider, M., García, O. E., and Sepúlveda, E.: TCCON data from Izaña (ES), Release GGG2014.R1, <https://doi.org/10.14291/tccon.ggg2014.izana01.r1>, 2017.

Boesch, H., Deutscher, N. M., Warneke, T., Byckling, K., Cogan, A. J., Griffith, D. W. T., Notholt, J., Parker, R. J., and Wang, Z.: $\text{HDO}/\text{H}_2\text{O}$ ratio retrievals from GOSAT, *Atmos. Meas. Tech.*, 6, 599–612, <https://doi.org/10.5194/amt-6-599-2013>, 2013.

275 Borsdorff, T., Hasekamp, O. P., Wassmann, A., and Landgraf, J.: Insights into Tikhonov regularization: application to trace gas column retrieval and the efficient calculation of total column averaging kernels, *Atmos. Meas. Tech.*, 7, 523–535, <https://doi.org/10.5194/amt-7-523-2014>, 2014.

Copernicus Climate Service: online, <https://climate.copernicus.eu/dry-and-warm-spring-and-summer>, vis 21 May 2019, 2018.

Coplen, T. B.: Guidelines and recommended terms for expression of stable-isotope-ratio and gas-ratio measurement results, *Rapid Commun. Mass Spectrom.*, 25, 2538–2560, <https://doi.org/10.1002/rcm.5129>, 2011.

280 Craig, H. and Gordon, L. I.: Deuterium and oxygen 18 variations in the ocean and the marine atmosphere, in: *Stable Isotopes in Oceanographic Studies and Paleotemperatures*, edited by Tongiorgi, E., pp. 9–130, Laboratorio di geologia nucleare, Pisa, 1965.

Dansgaard, W.: Stable isotopes in precipitation, *Tellus*, 16, 436–468, <https://doi.org/10.3402/tellusa.v16i4.8993>, 1964.

285 De Mazière, M., Thompson, A. M., Kurylo, M. J., Wild, J. D., Bernhard, G., Blumenstock, T., Braathen, G. O., Hannigan, J. W., Lambert, J.-C., Leblanc, T., McGee, T. J., Nedoluha, G., Petropavlovskikh, I., Seckmeyer, G., Simon, P. C., Steinbrecht, W., and Strahan, S. E.: The Network for the Detection of Atmospheric Composition Change (NDACC): history, status and perspectives, *Atmos. Chem. Phys.*, 18, 4935–4964, <https://doi.org/10.5194/acp-18-4935-2018>, 2018.

Deutscher, N. M., Notholt, J., Messerschmidt, J., Weinzierl, C., Warneke, T., Petri, C., and Grupe, P.: TCCON data from Bialystok (PL), Release GGG2014.R1, <https://doi.org/10.14291/tccon.ggg2014.bialystok01.r1/1183984>, 2015.

Dyroff, C., Fütterer, D., and Zahn, A.: Compact diode-laser spectrometer ISOWAT for highly sensitive airborne measurements of water-isotope ratios, *Applied Physics B*, 98, 537–548, <https://doi.org/10.1007/s00340-009-3775-6>, 2010.

290 Dyroff, C., Sanati, S., Christner, E., Zahn, A., Balzer, M., Bouquet, H., McManus, J. B., González-Ramos, Y., and Schneider, M.: Airborne in situ vertical profiling of HDO / $H_2^{16}O$ in the subtropical troposphere during the MUSICA remote sensing validation campaign, *Atmos. Meas. Tech.*, 8, 2037–2049, <https://doi.org/10.5194/amt-8-2037-2015>, 2015.

Frankenberg, C., Yoshimura, K., Warneke, T., Aben, I., Butz, A., Deutscher, N., Griffith, D., Hase, F., Notholt, J., Schneider, M., Schrijver, H., and Röckmann, T.: Dynamic Processes Governing Lower-Tropospheric HDO/ H_2O Ratios as Observed from Space and Ground, *Science*, 295, 325, 1374–1377, <https://doi.org/10.1126/science.1173791>, 2009.

Frankenberg, C., Wunch, D., Toon, G. C., Risi, C., Scheepmaker, R., Lee, J.-E., Wennberg, P. O., and Worden, J.: Water vapor isotopologue retrievals from high-resolution GOSAT shortwave infrared spectra, *Atmos. Meas. Tech.*, 6, 263–274, <https://doi.org/10.5194/amt-6-263-2013>, 2013.

González, Y., Schneider, M., Dyroff, C., Rodríguez, S., Christner, E., García, O. E., Cuevas, E., Bustos, J. J., Ramos, R., Guirado-Fuentes, 300 C., Barthlott, S., Wiegele, A., and Sepúlveda, E.: Detecting moisture transport pathways to the subtropical North Atlantic free troposphere using paired H_2O - δD in situ measurements, *Atmos. Chem. Phys.*, 16, 4251–4269, <https://doi.org/10.5194/acp-16-4251-2016>, 2016.

Gordon, I., Rothman, L., Hill, C., Kochanov, R., Tan, Y., Bernath, P., Birk, M., Boudon, V., Campargue, A., Chance, K., Drouin, B., Flaud, J.-M., Gamache, R., Hodges, J., Jacquemart, D., Perevalov, V., Perrin, A., Shine, K., Smith, M.-A., Tennyson, J., Toon, G., Tran, H., Tyuterev, V., Barbe, A., Császár, A., Devi, V., Furtenbacher, T., Harrison, J., Hartmann, J.-M., Jolly, A., Johnson, T., Karman, T., 305 Kleiner, I., Kyuberis, A., Loos, J., Lyulin, O., Massie, S., Mikhailenko, S., Moazzen-Ahmadi, N., Müller, H., Naumenko, O., Nikitin, A., Polyansky, O., Rey, M., Rotger, M., Sharpe, S., Sung, K., Starikova, E., Tashkun, S., Auwera, J. V., Wagner, G., Wilzewski, J., Wcisło, P., Yu, S., and Zak, E.: The HITRAN2016 molecular spectroscopic database, *J. Quant. Spectrosc. Radiat. Transfer*, 203, 3–69, <https://doi.org/10.1016/j.jqsrt.2017.06.038>, 2017.

Griffith, D. W., Velazco, V. A., Deutscher, N. M., Paton-Walsh, C., Jones, N. B., Wilson, S. R., Macatangay, R. C., Kettlewell, G. C., Buchholz, R. R., and Rigganbach, M. O.: TCCON data from Wollongong (AU), Release GGG2014.R0, 310 <https://doi.org/10.14291/tccon.ggg2014.wollongong01.r0/1149291>, 2014.

Gubler, S., Scherrer, S., Bader, S., Burgstall, A., Casanueva, A., Duguay-Tetzlaff, A., Gehrig, R., Kotlarski, S., and Spirig, C.: Hitze und Trockenheit im Sommerhalbjahr 2018 – eine klimatologische Übersicht, *Fachbericht MeteoSchweiz* 272, MeteoSchweiz, https://www.meteoschweiz.admin.ch/content/dam/meteoswiss/de/service-und-publikationen/Publikationen/doc/Fachbericht_TrockenheitHitze_2018_final_d.pdf, vis 7 Jun 2019, 2018.

Harries, J. E.: Atmospheric radiation and atmospheric humidity, *Quart. J. Roy. Meteor. Soc.*, 123, 2173–2186, <https://doi.org/10.1002/qj.49712354402>, 1997.

Hase, F., Blumenstock, T., Dohe, S., Groß, J., and Kiel, M.: TCCON data from Karlsruhe (DE), Release GGG2014.R1, <https://doi.org/10.14291/tccon.ggg2014.karlsruhe01.r1/1182416>, 2015.

320 Herbin, H., Hurtmans, D., Clerbaux, C., Clarisse, L., and Coheur, P.-F.: $H_2^{16}O$ and HDO measurements with IASI/MetOp, *Atmos. Chem. Phys.*, 9, 9433–9447, <https://doi.org/10.5194/acp-9-9433-2009>, 2009.

Herman, R. L., Cherry, J. E., Young, J., Welker, J. M., Noone, D., Kulawik, S. S., and Worden, J.: Aircraft validation of Aura Tropospheric Emission Spectrometer retrievals of HDO / H_2O , *Atmos. Meas. Tech.*, 7, 3127–3138, <https://doi.org/10.5194/amt-7-3127-2014>, 2014.

Hoffmann, G., Werner, M., and Heimann, M.: Water isotope module of the ECHAM atmospheric general circulation model: A study on 325 timescales from days to several years, *J. Geophys. Res.*, 103, 16 871–16 896, <https://doi.org/10.1029/98JD00423>, 1998.

Hu, H., Landgraf, J., Detmers, R., Borsdorff, T., Aan de Brugh, J., Aben, I., Butz, A., and Hasekamp, O.: Toward Global Mapping of Methane With TROPOMI: First Results and Intersatellite Comparison to GOSAT, *Geophys. Res. Lett.*, 45, 3682–3689, <https://doi.org/10.1002/2018GL077259>, 2018.

Iraci, L. T., Podolske, J. R., Hillyard, P. W., Roehl, C., Wennberg, P. O., Blavier, J.-F., Landeros, J., Allen, N., Wunch, D., Zavaleta, J.,
 330 Quigley, E., Osterman, G. B., Albertson, R., Dunwoody, K., and Boyden, H.: TCCON data from Edwards (US), Release GGG2014.R1, <https://doi.org/10.14291/tcccon.ggg2014.edwards01.r1/1255068>, 2016.

Joussaume, S., Sadourny, R., and Jouzel, J.: A general circulation model of water isotope cycles in the atmosphere, *Nature*, 311, 24–29, <https://doi.org/10.1038/311024a0>, 1984.

Kawakami, S., Ohyama, H., Arai, K., Okumura, H., Taura, C., Fukamachi, T., and Sakashita, M.: TCCON data from Saga (JP), Release
 335 GGG2014.R0, <https://doi.org/10.14291/tcccon.ggg2014.saga01.r0/1149283>, 2014.

Kiehl, J. T. and Trenberth, K. E.: Earth's Annual Global Mean Energy Budget, *Bull. Amer. Meteor. Soc.*, 78, 197–208, [https://doi.org/10.1175/1520-0477\(1997\)078<0197:EAGMEB>2.0.CO;2](https://doi.org/10.1175/1520-0477(1997)078<0197:EAGMEB>2.0.CO;2), 1997.

Kivi, R., Heikkinen, P., and Kyrö, E.: TCCON data from Sodankylä (FI), Release GGG2014.R0, <https://doi.org/10.14291/tcccon.ggg2014.sodankyla01.r0/1149280>, 2014.

340 Krol, M., Houweling, S., Bregman, B., van den Broek, M., Segers, A., van Velthoven, P., Peters, W., Dentener, F., and Bergamaschi, P.: The two-way nested global chemistry-transport zoom model TM5: algorithm and applications, *Atmos. Chem. Phys.*, 5, 417–432, <https://doi.org/10.5194/acp-5-417-2005>, 2005.

Lacour, J.-L., Risi, C., Clarisse, L., Bony, S., Hurtmans, D., Clerbaux, C., and Coheur, P.-F.: Mid-tropospheric δ D observations from IASI/MetOp at high spatial and temporal resolution, *Atmos. Chem. Phys.*, 12, 10 817–10 832, <https://doi.org/10.5194/acp-12-10817-2012>,
 345 2012.

Lacour, J.-L., Flamant, C., Risi, C., Clerbaux, C., and Coheur, P.-F.: Importance of the Saharan heat low in controlling the North Atlantic free tropospheric humidity budget deduced from IASI δ D observations, *Atmos. Chem. Phys.*, 17, 9645–9663, <https://doi.org/10.5194/acp-17-9645-2017>, 2017.

Landgraf, J., aan de Brugh, J., Scheepmaker, R., Borsdorff, T., Hu, H., Houweling, S., Butz, A., Aben, I., and Hasekamp, O.:
 350 Carbon monoxide total column retrievals from TROPOMI shortwave infrared measurements, *Atmos. Meas. Tech.*, 9, 4955–4975, <https://doi.org/10.5194/amt-9-4955-2016>, 2016.

Morino, I., Matsuzaki, T., and Horikawa, M.: TCCON data from Tsukuba (JP), 125HR, Release GGG2014.R2, <https://doi.org/10.14291/tcccon.ggg2014.tsukuba02.r2>, 2018a.

Morino, I., Yokozeki, N., Matsuzaki, T., and Horikawa, M.: TCCON data from Rikubetsu (JP), Release GGG2014.R2,
 355 <https://doi.org/10.14291/tcccon.ggg2014.rikubetsu01.r2>, 2018b.

Noone, D.: Pairing Measurements of the Water Vapor Isotope Ratio with Humidity to Deduce Atmospheric Moistening and Dehydration in the Tropical Midtroposphere, *J. Climate*, 25, 4476–4494, <https://doi.org/10.1175/JCLI-D-11-00582.1>, 2012.

Notholt, J., Petri, C., Warneke, T., Deutscher, N. M., Palm, M., Buschmann, M., Weinzierl, C., Macatangay, R. C., and Grupe, P.: TCCON data from Bremen (DE), Release GGG2014.R0, <https://doi.org/10.14291/tcccon.ggg2014.bremen01.r0/1149275>, 2014.

360 Notholt, J., Warneke, T., Petri, C., Deutscher, N. M., Weinzierl, C., Palm, M., and Buschmann, M.: TCCON data from Ny Ålesund, Spitsbergen (NO), Release GGG2014.R0, <https://doi.org/10.14291/tcccon.ggg2014.nyalesund01.r0/1149278>, 2017.

Payne, V. H., Noone, D., Dudhia, A., Piccolo, C., and Grainger, R. G.: Global satellite measurements of HDO and implications for understanding the transport of water vapour into the stratosphere, Quart. J. Roy. Meteor. Soc., 133, 1459–1471, <https://doi.org/10.1002/qj.127>, 2007.

365 Pfahl, S. and Wernli, H.: Quantifying the relevance of atmospheric blocking for co-located temperature extremes in the Northern Hemisphere on (sub-)daily time scales, Geophysical Research Letters, 39, <https://doi.org/10.1029/2012GL052261>, 2012.

Pfahl, S., Wernli, H., and Yoshimura, K.: The isotopic composition of precipitation from a winter storm – a case study with the limited-area model COSMO_{iso}, Atmos. Chem. Phys., 12, 1629–1648, <https://doi.org/10.5194/acp-12-1629-2012>, 2012.

Pollard, D. F., Robinson, J., and Shiona, H.: TCCON data from Lauder (NZ), Release GGG2014.R0, 370 <https://doi.org/10.14291/tccon.ggg2014.lauder03.r0>, 2019.

Rast, M., Johannessen, J., and Mauser, W.: Review of Understanding of Earth's Hydrological Cycle: Observations, Theory and Modelling, Surv. Geophys., 35, 491–513, <https://doi.org/10.1007/s10712-014-9279-x>, 2014.

Rayleigh, J. W. S.: On the distillation of binary mixtures, Philos. Mag., 4, 521–537, <https://doi.org/10.1080/14786440209462876>, 1902.

Rinsland, C. P., Goldman, A., Devi, V. M., Fridovich, B., Snyder, D. G. S., Jones, G. D., Murcray, F. J., Murcray, D. G., Smith, M. A. H., 375 Seals, R. K., Coffey, M. T., and Mankin, W. G.: Simultaneous stratospheric measurements of H₂O, HDO, and CH₄ from balloon-borne and aircraft infrared solar absorption spectra and tunable diode laser laboratory spectra of HDO, J. Geophys. Res., 89, 7259–7266, <https://doi.org/10.1029/JD089iD05p07259>, 1984.

Risi, C., Bony, S., Vimeux, F., and Jouzel, J.: Water-stable isotopes in the LMDZ4 general circulation model: Model evaluation for present-day and past climates and applications to climatic interpretations of tropical isotopic records, J. Geophys. Res., 115, 380 <https://doi.org/10.1029/2009JD013255>, 2010.

Rodgers, C. D.: Inverse methods for atmospheric sounding: theory and practice, vol. 2 of *Series on atmospheric, oceanic and planetary physics*, World Scientific, Singapore, 2000.

Rozanski, K. and Sonntag, C.: Vertical distribution of deuterium in atmospheric water vapour, Tellus, 34, 135–141, <https://doi.org/10.3402/tellusa.v34i2.10795>, 1982.

385 Scheepmaker, R. A., Frankenberg, C., Deutscher, N. M., Schneider, M., Barthlott, S., Blumenstock, T., Garcia, O. E., Hase, F., Jones, N., Mahieu, E., Notholt, J., Velazco, V., Landgraf, J., and Aben, I.: Validation of SCIAMACHY HDO/H₂O measurements using the TCCON and NDACC-MUSICA networks, Atmos. Meas. Tech., 8, 1799–1818, <https://doi.org/10.5194/amt-8-1799-2015>, 2015.

Scheepmaker, R. A., aan de Brugh, J., Hu, H., Borsdorff, T., Frankenberg, C., Risi, C., Hasekamp, O., Aben, I., and Landgraf, J.: HDO and H₂O total column retrievals from TROPOMI shortwave infrared measurements, Atmos. Meas. Tech., 9, 3921–3937, 390 <https://doi.org/10.5194/amt-9-3921-2016>, 2016.

Schneider, A., Borsdorff, T., aan de Brugh, J., Hu, H., and Landgraf, J.: A full-mission data set of H₂O and HDO columns from SCIAMACHY 2.3 μ m reflectance measurements, Atmos. Meas. Tech., 11, 3339–3350, <https://doi.org/10.5194/amt-11-3339-2018>, 2018.

Schneider, M. and Hase, F.: Optimal estimation of tropospheric H₂O and δ D with IASI/METOP, Atmos. Chem. Phys., 11, 11 207–11 220, <https://doi.org/10.5194/acp-11-11207-2011>, 2011.

395 Schneider, M., González, Y., Dyroff, C., Christner, E., Wiegele, A., Barthlott, S., García, O. E., Sepúlveda, E., Hase, F., Andrey, J., Blumenstock, T., Guirado, C., Ramos, R., and Rodríguez, S.: Empirical validation and proof of added value of MUSICA's tropospheric {H₂O, δ D} remote sensing products, Atmos. Meas. Tech., 8, 483–503, <https://doi.org/10.5194/amt-8-483-2015>, 2015.

Schneider, M., Wiegele, A., Barthlott, S., González, Y., Christner, E., Dyroff, C., García, O. E., Hase, F., Blumenstock, T., Sepúlveda, E., Mengistu Tsidu, G., Takele Kenea, S., Rodríguez, S., and Andrey, J.: Accomplishments of the MUSICA project to provide accurate,

400 long-term, global and high-resolution observations of tropospheric {H₂O,δD} pairs – a review, *Atmos. Meas. Tech.*, 9, 2845–2875, <https://doi.org/10.5194/amt-9-2845-2016>, 2016.

Sherlock, V., Connor, B., Robinson, J., Shiona, H., Smale, D., and Pollard, D. F.: TCCON data from Lauder (NZ), 125HR, Release GGG2014.R0, <https://doi.org/10.14291/tccon.ggg2014.lauder02.r0/1149298>, 2014.

Siddans, R.: S5P-NPP Cloud Processor ATBD, Tech. rep., Rutherford Appleton Laboratory, http://www.tropomi.eu/sites/default/files/files/S5P-NPPC-RAL-ATBD-0001_NPP-Clouds_v1p0p0_20160212.pdf, 2016.

405 Sodemann, H., Aemisegger, F., Pfahl, S., Bitter, M., Corsmeier, U., Feuerle, T., Graf, P., Hankers, R., Hsiao, G., Schulz, H., Wieser, A., and Wernli, H.: The stable isotopic composition of water vapour above Corsica during the HyMeX SOP1 campaign: insight into vertical mixing processes from lower-tropospheric survey flights, *Atmos. Chem. Phys.*, 17, 6125–6151, <https://doi.org/10.5194/acp-17-6125-2017>, 2017.

410 Steinwagner, J., Milz, M., von Clarmann, T., Glatthor, N., Grabowski, U., Höpfner, M., Stiller, G. P., and Röckmann, T.: HDO measurements with MIPAS, *Atmos. Chem. Phys.*, 7, 2601–2615, <https://doi.org/10.5194/acp-7-2601-2007>, 2007.

Stevens, B. and Bony, S.: What Are Climate Models Missing?, *Science*, 340, 1053–1054, <https://doi.org/10.1126/science.1237554>, 2013.

Strong, K., Roche, S., Franklin, J. E., Mendonca, J., Lutsch, E., Weaver, D., Fogal, P. F., Drummond, J. R., Batchelor, R., and Lindenmaier, R.: TCCON data from Eureka (CA), Release GGG2014.R3, <https://doi.org/10.14291/tccon.ggg2014.eureka01.r3>, 2019.

415 Té, Y., Jeseck, P., and Janssen, C.: TCCON data from Paris (FR), Release GGG2014.R0, <https://doi.org/10.14291/tccon.ggg2014.paris01.r0/1149279>, 2014.

Trigo, R. M., Trigo, I. F., DaCamara, C. C., and Osborn, T. J.: Climate impact of the European winter blocking episodes from the NCEP/NCAR Reanalyses, *Climate Dyn.*, 23, 17–28, <https://doi.org/10.1007/s00382-004-0410-4>, 2004.

420 Veefkind, J., Aben, I., McMullan, K., Förster, H., de Vries, J., Otter, G., Claas, J., Eskes, H., de Haan, J., Kleipool, Q., van Weele, M., Hasekamp, O., Hoogeveen, R., Landgraf, J., Snel, R., Tol, P., Ingmann, P., Voors, R., Kruizinga, B., Vink, R., Visser, H., and Levelt, P.: TROPOMI on the ESA Sentinel-5 Precursor: A GMES mission for global observations of the atmospheric composition for climate, air quality and ozone layer applications, *Remote Sens. Environ.*, 120, 70–83, <https://doi.org/10.1016/j.rse.2011.09.027>, 2012.

Warneke, T., Messerschmidt, J., Notholt, J., Weinzierl, C., Deutscher, N. M., Petri, C., and Grupe, P.: TCCON data from Orléans (FR), Release GGG2014.R0, <https://doi.org/10.14291/tccon.ggg2014.orleans01.r0/1149276>, 2019.

425 Weaver, D.: Water Vapour Measurements in the Canadian High Arctic, phdthesis, University of Toronto, <http://hdl.handle.net/1807/95942>, 2019.

Wen, X.-F., Zhang, S.-C., Sun, X.-M., Yu, G.-R., and Lee, X.: Water vapor and precipitation isotope ratios in Beijing, China, *J. Geophys. Res.*, 115, <https://doi.org/10.1029/2009JD012408>, d01103, 2010.

Wennberg, P. O., Roehl, C. M., Blavier, J.-F., Wunch, D., and Allen, N. T.: TCCON data from Jet Propulsion Laboratory (US), 2011, Release GGG2014.R1, <https://doi.org/10.14291/tccon.ggg2014.jpl02.r1/1330096>, 2014.

430 Wennberg, P. O., Wunch, D., Roehl, C. M., Blavier, J.-F., Toon, G. C., and Allen, N. T.: TCCON data from Caltech (US), Release GGG2014.R1, <https://doi.org/10.14291/tccon.ggg2014.pasadena01.r1/1182415>, 2015.

Wennberg, P. O., Wunch, D., Roehl, C. M., Blavier, J.-F., Toon, G. C., and Allen, N. T.: TCCON data from Lamont (US), Release GGG2014.R1, <https://doi.org/10.14291/tccon.ggg2014.lamont01.r1/1255070>, 2016.

435 Wennberg, P. O., Roehl, C. M., Wunch, D., Toon, G. C., Blavier, J.-F., Washenfelder, R., Keppel-Aleks, G., Allen, N. T., and Ayers, J.: TCCON data from Park Falls (US), Release GGG2014.R1, <https://doi.org/10.14291/tccon.ggg2014.parkfalls01.r1>, 2017.

Worden, J., Bowman, K., Noone, D., Beer, R., Clough, S., Eldering, A., Fisher, B., Goldman, A., Gunson, M., Herman, R., Kulawik, S. S., Lampel, M., Luo, M., Osterman, G., Rinsland, C., Rodgers, C., Sander, S., Shephard, M., and Worden, H.: Tropospheric Emission Spectrometer observations of the tropospheric HDO/H₂O ratio: Estimation approach and characterization, *J. Geophys. Res.*, 111, 440 <https://doi.org/10.1029/2005JD006606>, d16309, 2006.

Worden, J., Noone, D., Bowman, K., science team, T. T. E. S., and data contributors: Importance of rain evaporation and continental convection in the tropical water cycle, *Nature*, 445, 528, <https://doi.org/10.1038/nature05508>, 2007.

Worden, J. R., Kulawik, S. S., Fu, D., Payne, V. H., Lipton, A. E., Polonsky, I., He, Y., Cady-Pereira, K., Moncet, J.-L., Herman, R. L., Irion, F. W., and Bowman, K. W.: Characterization and evaluation of AIRS-based estimates of the deuterium content of water vapor, *Atmos. Meas. Tech.*, 12, 2331–2339, <https://doi.org/10.5194/amt-12-2331-2019>, 2019.

445 Wunch, D., Toon, G. C., Blavier, J.-F. L., Washenfelder, R. A., Notholt, J., Connor, B. J., Griffith, D. W. T., Sherlock, V., and Wennberg, P. O.: The Total Carbon Column Observing Network, *Philos. T. Roy. Soc. A*, 369, 2087–2112, <https://doi.org/10.1098/rsta.2010.0240>, 2011.

Wunch, D., Toon, G. C., Sherlock, V., Deutscher, N. M., Liu, X., Feist, D. G., and Wennberg, P. O.: The Total Carbon Column Observing 450 Network's GGG2014 Data Version, Tech. rep., TCCON, <https://doi.org/10.14291/tccon.ggg2014.documentation.R0/1221662>, 2015.

Wunch, D., Mendonca, J., Colebatch, O., Allen, N. T., Blavier, J.-F., Roche, S., Hedelius, J., Neufeld, G., Springett, S., Worthy, D., Kessler, R., and Strong, K.: TCCON data from East Trout Lake, SK (CA), Release GGG2014.R1, <https://doi.org/10.14291/tccon.ggg2014.easttroutlake01.r1>, 2018.

Yoshimura, K., Kanamitsu, M., Noone, D., and Oki, T.: Historical isotope simulation using Reanalysis atmospheric data, *J. Geophys. Res.*, 455 113, <https://doi.org/10.1029/2008JD010074>, 2008.

Zakharov, V. I., Imasu, R., Gribanov, K. G., Hoffmann, G., and Jouzel, J.: Latitudinal distribution of the deuterium to hydrogen ratio in the atmospheric water vapor retrieved from IMG/ADEOS data, *Geophys. Res. Lett.*, 31, <https://doi.org/10.1029/2004GL019433>, 112104, 2004.